



RESEARCH ARTICLE

A one-DOF compliant gripper mechanism with four identical twofold-symmetric Bricard linkages

Kunjing Chen^{1, #}, Tianxiang Lai^{1, #}, Fufu Yang^{1, 2, * }, Jun Zhang^{1, 2 } and Ligang Yao^{1, 2}

¹School of Mechanical Engineering and Automation, Fuzhou University, Fuzhou, 350108, China and ²Fujian Province Digital Design Center for Manufacturing, Fuzhou, Fujian, 350108, China

*Corresponding author. E-mail: yangfufu@fzu.edu.cn

Received: 14 February 2022; **Revised:** 19 September 2022; **Accepted:** 25 September 2022;

First published online: 27 October 2022

Keywords: one-DOF gripper, twofold-symmetric Bricard linkages, truss-transformation method, SVD, overconstrained linkage, deployable structure

Abstract

Gripper is one of the most important parts of robot because of contacting with workpieces directly and has attracted lots of research interests. However, the existing grippers are either simple in function or complex in structure. In this paper, we will propose a one-DOF gripper based on a compliant mechanism with four identical twofold-symmetric Bricard linkages. A mobile network with four identical twofold-symmetric Bricard linkages with particular design parameters is constructed at first. Kinematics, such as mobility, singularity, and folding performance, is then analyzed to show the potential of realizing the function of grasping. The result is demonstrated with a physical prototype. To simplify the fabricating process, a compliant mechanism of the network is designed and fabricated with a single polypropylene board, and the grasping function is realized by a cable-driven scheme. Some grasping experiments are carried out on different types of objects which shows that the proposed and fabricated four-figure gripper is simple in structure and has a great grasping function. The work provides a new idea for the design of grippers with low cost, simple structure, and rich functions.

1. Introduction

In robot, gripper is one of the most commonly used end effectors since it can grasp different types of objects tightly for potential applications and hence have attracted many research interests while being widely used in practical applications [1–3]. Among the design and realization of grippers, there are two of the most important issues. The first one is to let the grippers fit different rigidity, and the second one is to fit different shapes.

For the first issue, some adaptive control algorithms are introduced. For instance, Maggi *et al.* [4] proposed a novel adaptive underactuated vacuum gripper. Zhou *et al.* [5] developed an observer-based adaptive boundary iterative learning control method. Yang *et al.* [6] proposed an extreme learning machine based control scheme for uncertain robot manipulation or stopping performing tactile recognition. Mukherjee *et al.* [7] worked on a grasp optimization algorithm, for minimizing the net energy utilized by a five-fingered humanoid robotic hand for securing a precise grasp.

For the second issue, some flexible grippers with foldable and bionic structures were proposed in recent years [8]. For example, Abondance *et al.* [9] proposed a dexterous three-fingered soft robotic hand that can perform hand manipulations robustly in the presence of uncertainty. Park *et al.* [10] developed a hybrid gripper that combines soft and rigid components to simultaneously improve fingertip force and actuation speed. Zhang and Oseyemi [11] presented a new SPA with a herringbone chamber design, capable of combined longitudinal and transverse bending deformations that allow for improved

[#]Kunjing Chen and Tianxiang Lai contribute equally to the paper.

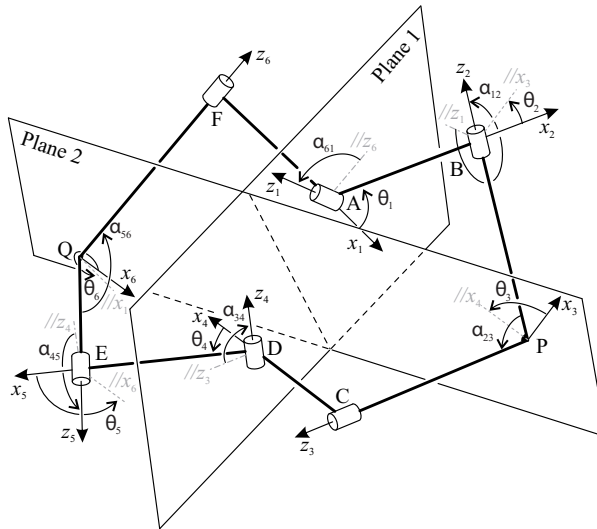


Figure 1. The twofold-symmetric Bricard linkage.

conformality in soft gripping. In the field of medicine, grippers with adjustable stiffness were also developed, such as a variable-stiffness robotic gripper by Cardin-Catalan *et al.* [12] and a foldable manipulator for minimally invasive surgery by Shang *et al.* [13]. Meanwhile, some origami patterns were adopted in the design of adaptive grippers due to the foldability with multi-DOF [14–17]. Moreover, underactuation is an important approach for simplified designs. Hota and Kumar [18] present a study on the effect of design parameters of an underactuated hand on its grasp performance. Su *et al.* [19] proposed a novel self-adaptive underactuated robot hand with rigid-flexible coupling fingers. Furthermore, Marwan *et al.* [20] presented a comprehensive review devoted to the techniques related to reaching and grasping objects in different workplaces.

However, these grippers are either assembled of many parts or require a complex-driven system, which is not conducive to reducing cost and ensuring reliability as well as stability. Fortunately, spatial overconstrained mechanisms [21] have the advantages of simple structure and good rigidity, which always provide solutions for simplified designs with large rigidity. Among the spatial overconstrained mechanisms, those with symmetric properties, such as Myard 5R linkage [22], line-symmetric 6R linkage [23], plane-symmetric Bricard 6R linkage [24], twofold-symmetric 6R linkage [25], threefold-symmetric 6R linkage [26], are preferred to be chosen in applications. Meanwhile, cable-driven is a convenient way to drive manipulators with simple structures [27]. Therefore, in this paper, we will choose a typical overconstrained linkage with great symmetric properties, twofold-symmetric Bricard 6R linkages [28] being easy to be fabricated in the compliant form, to construct a mobile network and to design a conceptual one-DOF compliant gripper.

The paper is organized as follows. In Section 2, the geometric conditions and characteristics of the twofold-symmetric Bricard 6R linkage are introduced. Section 3 is to construct the network with four identical twofold-symmetric Bricard 6R linkages, whose grasping potential is demonstrated by kinematic analysis and a physical prototype. In Section 4, a compliant gripper based on the proposed network is constructed, and the grasping function is realized with the help of a set of designed driven devices. Conclusions are drawn in Section 5.

2. Twofold-symmetric bricard linkage

Figure 1 shows a twofold-symmetric Bricard linkage, which is both plane-symmetric and line-symmetric one with six links and six revolute joints (R-joints). There are two symmetric planes, 1 and 2, for these

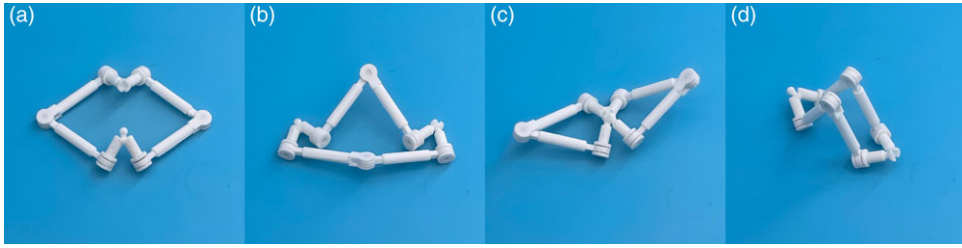


Figure 2. The prototype with parameters $\alpha = \frac{5\pi}{3}, \gamma = \frac{\pi}{3}, a = 60 \text{ mm}, r = 25 \text{ mm}$ at (a) twofold-symmetric 6R, (b) plane-symmetric 6R, (c) spherical 4R, and (d) two-bar modes.

links and joints. The geometric conditions are

$$\alpha_{61} = \alpha_{34} = \alpha, \alpha_{23} = \alpha_{56} = \beta = 2\pi - \alpha, \alpha_{12} = 2\pi - \alpha_{45} = \gamma, \tag{1a}$$

$$a_{12} = a_{45} = 0, a_{23} = a_{34} = a_{56} = a_{61} = a, \tag{1b}$$

$$R_1 = R_4 = r, R_2 = R_5 = -r$$

$$(|BP| = |CP| = |EQ| = |FQ| = r). \tag{1c}$$

The coordinate frames are set up by the D–H notation [29], where z_i is along the revolute axis of joint i ; x_i is the common normal direction pointing from z_{i-1} to z_i ; $a_{i(i+1)}$ is the normal distance between z_i and z_{i+1} ; $\alpha_{i(i+1)}$ is the angle of rotation from z_i to z_{i+1} about axis x_{i+1} ; R_i is the normal distance between x_i and x_{i+1} ; and θ_i is the angle of rotation from x_i and x_{i+1} about axis z_i . Here, a, r, α, γ are the geometrical parameters of the linkage, θ_i is the kinematic variable to show instantaneous configurations.

There are four possible motion modes for the linkage, i.e., twofold-symmetric 6R motion mode, plane-symmetric 6R motion mode, spherical 4R motion mode and two-bar mode, as shown in Fig. 2, and their kinematic equations [25] are as follows.

1. Twofold-symmetric 6R motion mode

$$\theta_5 = \theta_3, \theta_6 = \theta_2, \theta_4 = \theta_1, \theta_3 = \theta_2 + \pi, \tan \frac{\theta_1}{2} = \frac{D}{E}. \tag{2}$$

2. Plane-symmetric 6R motion mode

$$\theta_5 = \theta_3, \theta_6 = \theta_2, \tan \frac{\theta_3}{2} = \frac{C}{F}, \tan \frac{\theta_1}{2} = \frac{G}{H}, \tan \frac{\theta_4}{2} = \frac{I}{J}. \tag{3}$$

3. Spherical 4R motion mode

$$\sin \phi_{23} \sin \phi_{35} \cos \phi_{35} \cos (\theta_2 - \psi) - (\sin \phi_{23} \cos \phi_{35} + \cos \phi_{23} \sin \phi_{35} \cos (\theta_2 - \psi)) L_1 - \sin \phi_{35} \sin (\theta_2 - \psi) L_2 - \cos \phi_{23} \cos^2 \phi_{35} + \cos \phi_{23} = 0, \tag{4a}$$

$$\theta_5 = \theta_2 + \pi \text{ or } \theta_5 = 2\psi - \theta_2 + \pi, \tag{4b}$$

$$\sin \phi_{35} \sin \phi_{23} \cos \phi_{23} \cos (\theta_2 - \psi) + (\sin \phi_{23} \cos \phi_{23} \sin^2 \phi_{23} \cot \phi_{35} \cos (\theta_2 - \psi)) M_1 + \frac{\sin^2 \phi_{23}}{\sin \phi_{35}} \sin (\theta_2 - \psi) M_2 - \cos \phi_{35} \cos^2 \phi_{23} + \cos \phi_{35} = 0 \tag{4c}$$

in which $C, D, E, F, G, H, I, J, \phi_{23}, \phi_{35}, \psi, L_1, L_2, M_1,$ and M_2 can be found in [22].

4. Two-bar mode

When $\alpha \in \left(\frac{3\pi}{2}, 2\pi\right)$ and $2\alpha - \gamma = \pi + 2l_1\pi, l_1 \in Z,$

$$\theta_1 = \theta_4 = q_5, \theta_2 = \theta_6 = \pi, \theta_3 = \theta_5 = 0, q_5 \in [-\pi, \pi]. \tag{5}$$

When $\alpha \in \left(\pi, \frac{3\pi}{2}\right)$ and $2\alpha + \gamma = \pi + 2l_2\pi, l_2 \in Z,$

$$\theta_1 = \theta_4 = q_6, \theta_2 = \theta_6 = 0, \theta_3 = \theta_5 = \pi, q_6 \in [-\pi, \pi]. \tag{6}$$

When $\alpha = \frac{3\pi}{2}, \gamma \in (0, \pi), r \neq 0, a \in \forall,$ there is no two-bar mode.

Kinematic equations of twofold-symmetric 6R motion mode and two-bar mode show that the kinematic relationships are related to α and $\gamma,$ while a and r do not affect the folding properties.

3. The network of four identical twofold-symmetric bricard linkages

3.1. Construction of the network

The target of this paper is to design a compliant gripper mechanism [30] that does not need complicated assemblies. Milling polypropylene (PP) board, which always exhibits the property of good fatigue strength, is a common way to fabricate compliant mechanisms. Therefore, the directions of R -joints in complaint mechanisms are expected to be either parallel to the workpiece plane or perpendicular to the plane to facilitate manufacturing, see hinge D, F in Fig. 3(a). Then, $\frac{\pi}{2}$ and $\frac{3\pi}{2}$ are preferred to be chosen as the twist angles in the linkage.

Figure 3(a) shows a physical prototype of a twofold-symmetric Bricard linkage with twist angles $\alpha = \frac{3\pi}{2}$ and $\gamma = \frac{\pi}{2},$ whose schematic diagram is shown in Fig. 3(b). Due to the great symmetric property of the linkage, a network can be constructed by taking four identical units, distributing them as a 2×2 array, as shown in Fig. 3(c).

In this assembly, there are 17 links connected with 12 single R -joints, e.g., joints B, C, K, L, E, F, G, H, N, P, Q, and T, and four compound R -joints, e.g., joint A, D, J, and M. For a single R -joint, it can be realized easily by milling a thin strip, as shown in Fig. 3(a). However, for compound R -joints, it is difficult to manufacture since three thin strips, see three t_m in Fig. 3(d), could not coincide at one common position.

To facilitate the manufacturing of compliant compound R -joints, the network was modified by offsetting the adjacent Bricard units at A, D, J, and M with a distance $w,$ as shown in Fig. 4(a). According to the folding and unfolding characteristics of the network, the mechanism realizes the functions of unfolding and grasping through the cooperation of four Bricard mechanisms, among which a, b, c, and d on links 13, 14, 15, and 16 are 4 grasping points, the link 17 is the frame.

To evaluate the property of the mechanism, mobility and kinematics will be studied to show the potential as a gripper.

3.2. Mobility analysis

Figure 5(a) gives the topological graph of the proposed network [31], as shown in Fig. 4(a), by taking links as vertices, and joints as edges. There are four kinematic loops, I, II, III, and IV. Among them, the

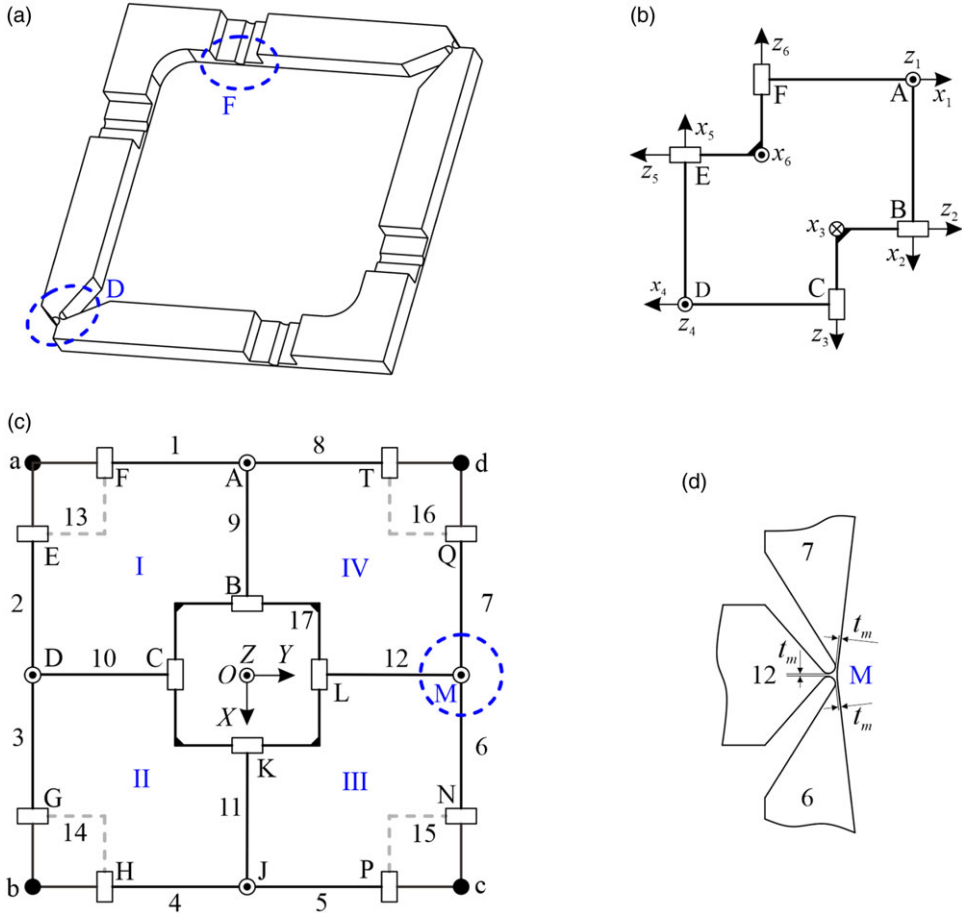


Figure 3. The construction of a network by (a) milling PP board to form a compliant linkage showing with (b) its schematic diagram. (c) The network is obtained by four units containing four (d) compound R-joints.

vertices (links) are labeled with numbers, and the edges (joints) with A, B, C, . . . T. The directed graph is given in Fig. 5(b) to show the four kinematic loops.

The global coordinate system $O\text{-}XYZ$ is established at the center of link 17 to evaluate its kinematic behaviors, where X axis directs along \vec{BK} , Y axis directs along \vec{CL} , and Z axis is determined by the right-hand rule, as shown in Fig. 4(a). Therefore, the coordinate values of all points are

$$\begin{aligned}
 A_1 &= \left(-n_3, -\frac{w}{2}, 0\right)^T & A_4 &= \left(-n_3, \frac{w}{2}, 0\right)^T & B &= (-n_2, 0, 0)^T & C &= (0, -n_2, 0)^T \\
 D_1 &= \left(-\frac{w}{2}, -n_3, 0\right)^T & D_2 &= \left(\frac{w}{2}, -n_3, 0\right)^T & E &= (-n_1, -n_3, 0)^T & F &= (-n_3, -n_1, 0)^T \\
 G &= (n_1, -n_3, 0)^T & H &= (n_3, -n_1, 0)^T & J_2 &= \left(n_3, -\frac{w}{2}, 0\right)^T & J_3 &= \left(n_3, \frac{w}{2}, 0\right)^T \\
 K &= (n_2, 0, 0)^T & L &= (0, n_2, 0)^T & M_3 &= \left(\frac{w}{2}, n_3, 0\right)^T & M_4 &= \left(-\frac{w}{2}, n_3, 0\right)^T \\
 N &= (n_1, n_3, 0)^T & P &= (n_3, n_1, 0)^T & Q &= (-n_1, n_3, 0)^T & T &= (-n_3, n_1, 0)^T
 \end{aligned} \tag{7}$$

where $n_1 = a + \frac{w}{2}$, $n_2 = r + \frac{w}{2}$, $n_3 = a + r + \frac{w}{2}$.

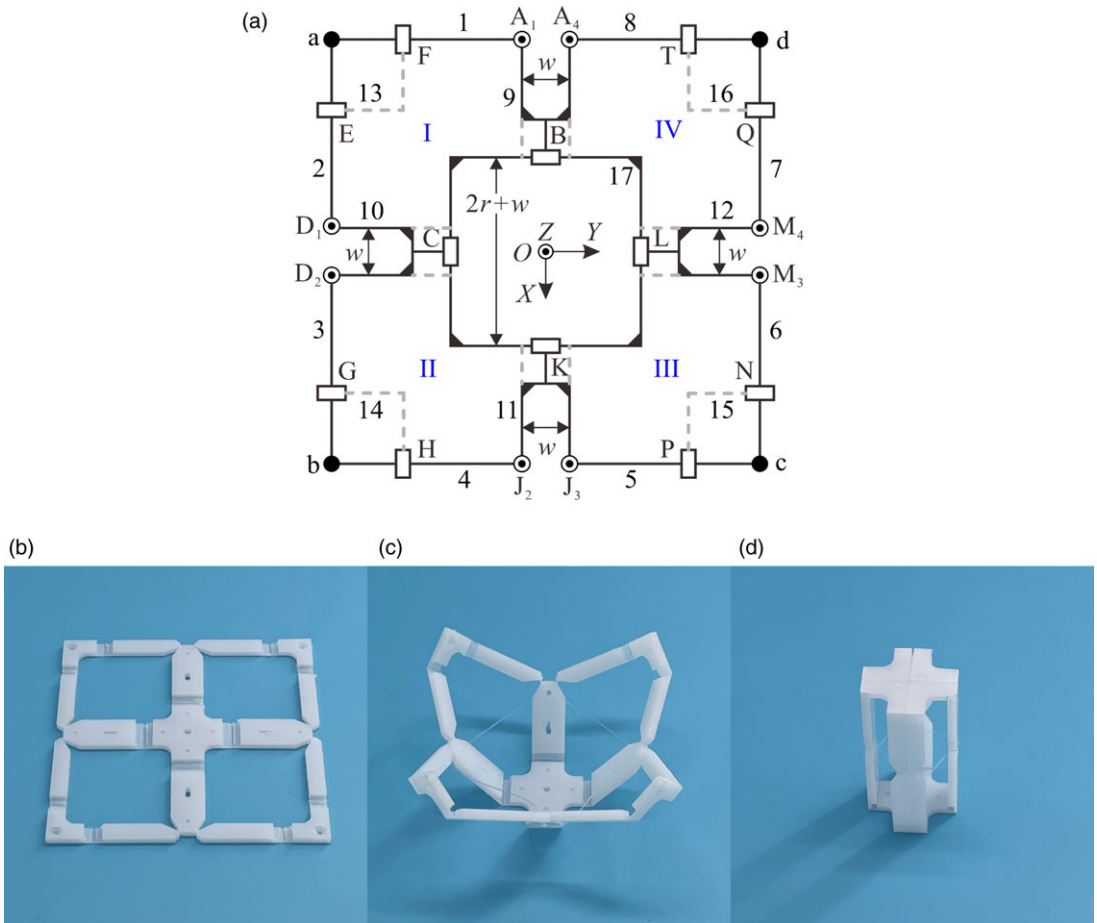


Figure 4. The compliant mechanism to construct a four-finger gripper with (a) structure diagram was manufactured with one PP board (a) at the plane configuration, (b) at the middle folding process, and (c) at the fully folded configuration.

At the planar configuration, the unit direction vectors of all joints are $s_1 = (1, 0, 0)^T, s_2 = (0, 1, 0)^T, s_3 = (1, 0, 0)^T$, where s_3 is the direction vectors of joints $A_1, A_4, D_1, D_2, J_2, J_3, M_3,$ and M_4, s_2 is that of joints $B, E, G, K, N,$ and Q, s_1 is for $C, F, H, L, P,$ and T . According to the definition of the screw [32]

$$\mathcal{S} = \begin{pmatrix} s_i \\ r \times s_i \end{pmatrix}, \tag{8}$$

the screws of the R -joints are,

$$\begin{aligned} \mathcal{S}_{A_1} &= (s_3, w/2, -n_3, 0)^T & \mathcal{S}_F &= (s_1, 0, 0, -n_1)^T & \mathcal{S}_{M_3} &= (s_3, -n_3, w/2, 0)^T \\ \mathcal{S}_{A_4} &= (s_3, -w/2, -n_3, 0)^T & \mathcal{S}_G &= (s_2, 0, 0, -n_1)^T & \mathcal{S}_{M_4} &= (s_3, -n_3, -w/2, 0)^T \\ \mathcal{S}_B &= (s_2, 0, 0, n_2)^T & \mathcal{S}_H &= (s_1, 0, 0, -n_1)^T & \mathcal{S}_N &= (s_2, 0, 0, -n_1)^T \\ \mathcal{S}_C &= (s_1, 0, 0, -n_2)^T & \mathcal{S}_{J_2} &= (s_3, w/2, n_3, 0)^T & \mathcal{S}_P &= (s_1, 0, 0, n_1)^T \\ \mathcal{S}_{D_1} &= (s_3, n_3, -w/2, 0)^T & \mathcal{S}_{J_3} &= (s_3, -w/2, n_3, 0)^T & \mathcal{S}_Q &= (s_2, 0, 0, n_1)^T \end{aligned} ,$$

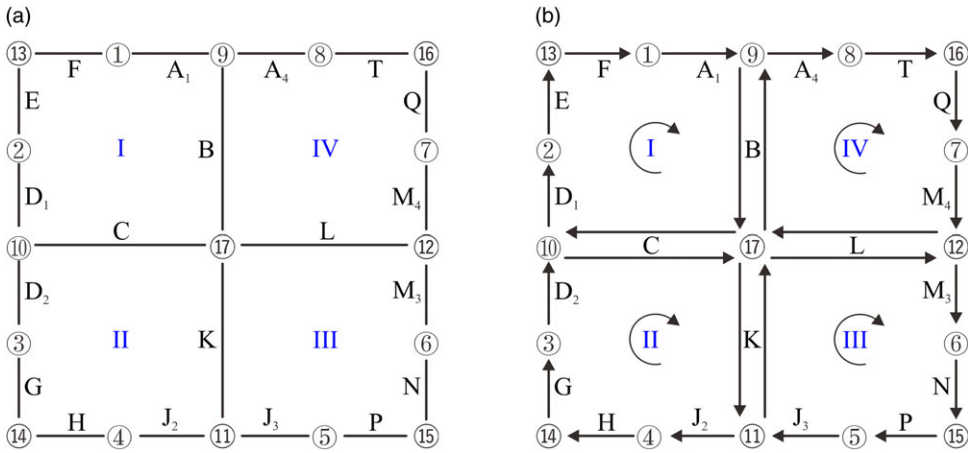


Figure 5. The topological graph of the proposed network by (a) taking links as vertices, joints as edges, and (b) its directed graph to show four kinematic loops.

$$\begin{aligned} \mathcal{S}_{D_2} &= (s_3, n_3, w/2, 0)^T & \mathcal{S}_K &= (s_2, 0, 0, -n_2)^T & \mathcal{S}_T &= (s_1, 0, 0, n_1)^T \\ \mathcal{S}_E &= (s_2, 0, 0, n_1)^T & \mathcal{S}_L &= (s_1, 0, 0, n_2)^T \end{aligned} \tag{9}$$

According to [31], the kinematic constraints are

$$\begin{aligned} \omega_{A_1} \mathcal{S}_{A_1} + \omega_B \mathcal{S}_B + \omega_C \mathcal{S}_C + \omega_{D_1} \mathcal{S}_{D_1} + \omega_E \mathcal{S}_E + \omega_F \mathcal{S}_F &= 0 \\ -\omega_C \mathcal{S}_C + \omega_{D_2} \mathcal{S}_{D_2} + \omega_G \mathcal{S}_G + \omega_H \mathcal{S}_H + \omega_{J_2} \mathcal{S}_{J_2} + \omega_K \mathcal{S}_K &= 0 \\ \omega_{J_3} \mathcal{S}_{J_3} - \omega_K \mathcal{S}_K + \omega_L \mathcal{S}_L + \omega_{M_3} \mathcal{S}_{M_3} + \omega_N \mathcal{S}_N + \omega_P \mathcal{S}_P &= 0 \\ \omega_{A_4} \mathcal{S}_{A_4} - \omega_B \mathcal{S}_B - \omega_L \mathcal{S}_L + \omega_{M_4} \mathcal{S}_{M_4} + \omega_Q \mathcal{S}_Q + \omega_T \mathcal{S}_T &= 0 \end{aligned} \tag{10}$$

where ω_i represents the angular velocity of R -joint i .

The equations can be written in the matrix form

$$\mathbf{K}_{24 \times 20} \cdot \boldsymbol{\omega}_{20 \times 1} = 0, \tag{11}$$

where $\boldsymbol{\omega}$ is the collection of velocities with a vector, $\mathbf{K}_{24 \times 20}$ is a coefficient matrix composed with screw values from Eqs. (11).

$$\boldsymbol{\omega} = [\omega_{A_1}, \omega_{A_4}, \omega_B, \omega_C, \omega_{D_1}, \omega_{D_2}, \omega_E, \omega_F, \omega_G, \omega_H, \omega_{J_2}, \omega_{J_3}, \omega_K, \omega_L, \omega_{M_3}, \omega_{M_4}, \omega_N, \omega_P, \omega_Q, \omega_T]^T$$

$$\mathbf{K}_{24 \times 20} = \begin{bmatrix} \mathcal{S}_{A_1}, 0, \mathcal{S}_B, \mathcal{S}_C, \mathcal{S}_{D_1}, 0, \mathcal{S}_E, \mathcal{S}_F, \bar{\mathbf{0}}_{1 \times 12}; \\ \bar{\mathbf{0}}_{1 \times 3}, -\mathcal{S}_C, 0, \mathcal{S}_{D_2}, 0, 0, \mathcal{S}_G, \mathcal{S}_H, \mathcal{S}_{J_2}, 0, \mathcal{S}_K, \bar{\mathbf{0}}_{1 \times 7}; \\ \bar{\mathbf{0}}_{1 \times 11}, \mathcal{S}_{J_3}, -\mathcal{S}_K, \mathcal{S}_L, \mathcal{S}_{M_3}, 0, \mathcal{S}_N, \mathcal{S}_P, 0, 0; \\ 0, \mathcal{S}_{A_4}, -\mathcal{S}_B, \bar{\mathbf{0}}_{1 \times 10}, -\mathcal{S}_L, \mathcal{S}_{M_4}, \bar{\mathbf{0}}_{1 \times 3}, \mathcal{S}_Q, \mathcal{S}_T; \end{bmatrix} \tag{12}$$

The mobility of the mechanism M should equal the dimension of the nullspace of $\mathbf{K}_{24 \times 20}$.

$$M = 20 - \text{rank}(\mathbf{K}_{24 \times 20}) = 20 - 19 = 1. \tag{13}$$

Therefore, the degree of freedom of the mechanism is one at this configuration.

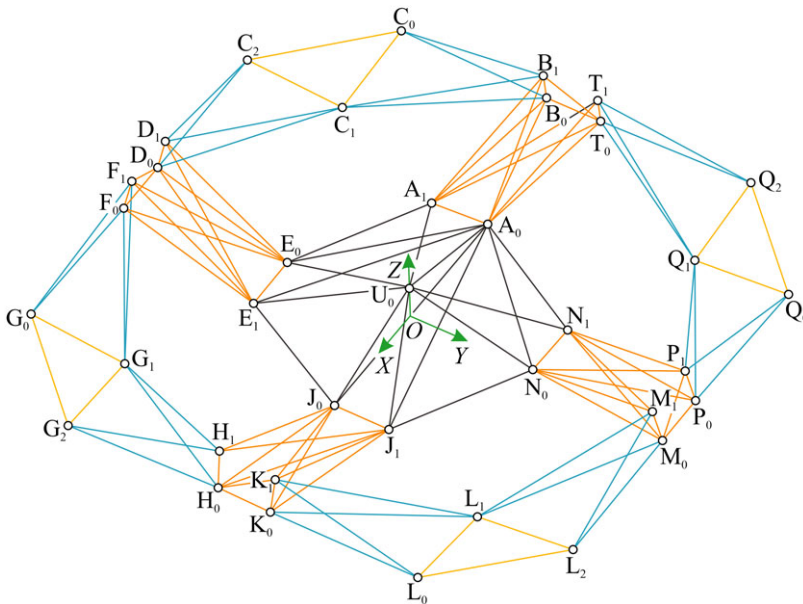


Figure 6. The truss form of the mechanism.

Since the unit of the mechanism, twofold-symmetric Bricard linkage, owns four possible motion modes being reconfigurable with some bifurcation points. The mobility and singularity analysis along the whole motion period will be analyzed in the following part.

3.3. Singularity analysis

The mechanism is equivalently transformed into the truss form by the truss-transformation method [33], see Fig. 6. In the proposed network, there are four types of links, e.g., BCKL, A_1A_4B , A_1F , and EF. They can be transformed as spatial polyhedron $A_0A_1E_0E_1J_0J_1N_0N_1U_0$, polyhedron $A_0A_1B_0B_1T_0T_1$, tetrahedron $B_0B_1C_0C_1$, and plane triangle $C_0C_1C_2$, respectively.

For the truss, there are $b = 110$ bars and $j = 34$ joints and its equilibrium equations [34] can be established conveniently by coordinate values of all vertices.

$$H \cdot t = f, \tag{14}$$

where H is the equilibrium matrix with dimensions 102×110 and can be obtained by Matlab according to ref. [34], t is the inner tensions along all bars, and f is the external force on all vertices. Here, we only consider the truss without external forces, i.e. $f = 0$. Then Eq. (15a) becomes a set of homogenous linear equations

$$H \cdot t = 0, \tag{15}$$

The instantaneous mobility is then obtained by the rank of H [34].

$$M = 3j - \text{rank}(H) - 6. \tag{16}$$

Meanwhile, the singular value decomposition (SVD) method is a convenient way to calculate the rank of a matrix. By a predictor and corrector strategy through SVD [35], the motion process of the truss form is obtained. The singularity property can be obtained by recording the singular values, as shown in Fig. 7(a). It can be found that the possible singular positions only occurred in the situations of physical interference illustrated with curves with gray on the left sides. To evaluate the potential of grasping further, the distances among four fingers, ab, bc, cd, da, ac, and bd are calculated in Fig. 7(b). It can be found that when θ_2^I approaches $\theta_{2f1}^I = -0.03\pi$ and $\theta_{2f2}^I = -0.97\pi$, the distances are both close

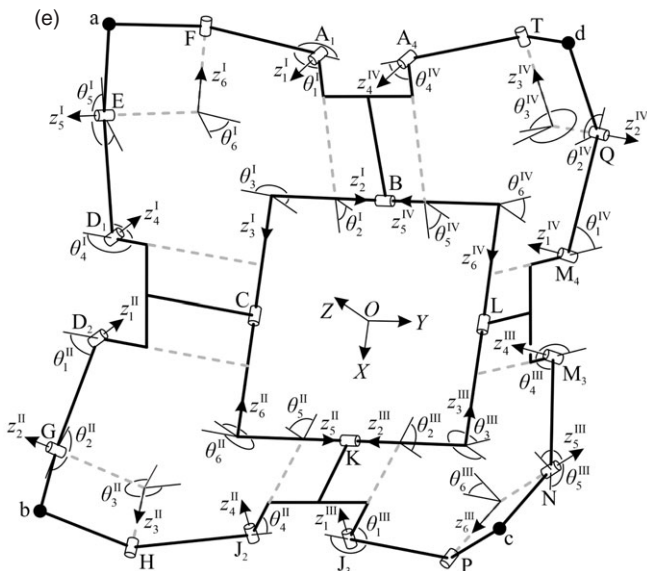
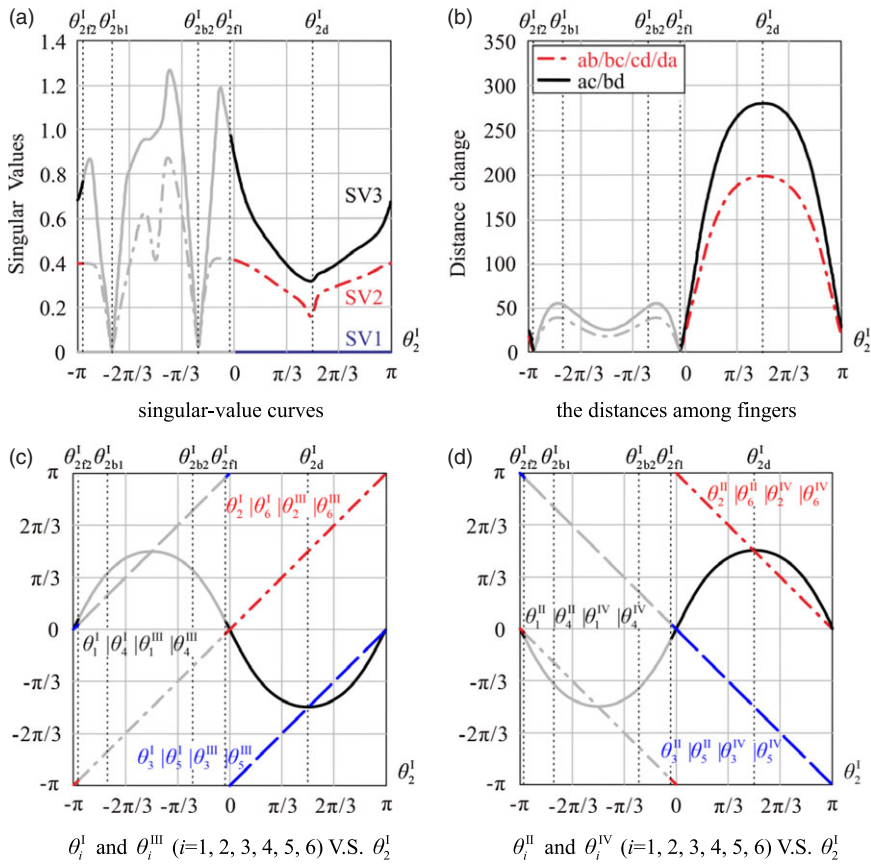


Figure 7. Kinematics of four-finger gripper. (a) singular-value curves. (b) the distances among fingers. (c) θ_i^I and θ_i^{III} ($i = 1, 2, 3, 4, 5, 6$) v.s. θ_2^I . (d) θ_i^{II} and θ_i^{IV} ($i = 1, 2, 3, 4, 5, 6$) v.s. θ_2^I . (e) schematic diagram of joint variables.

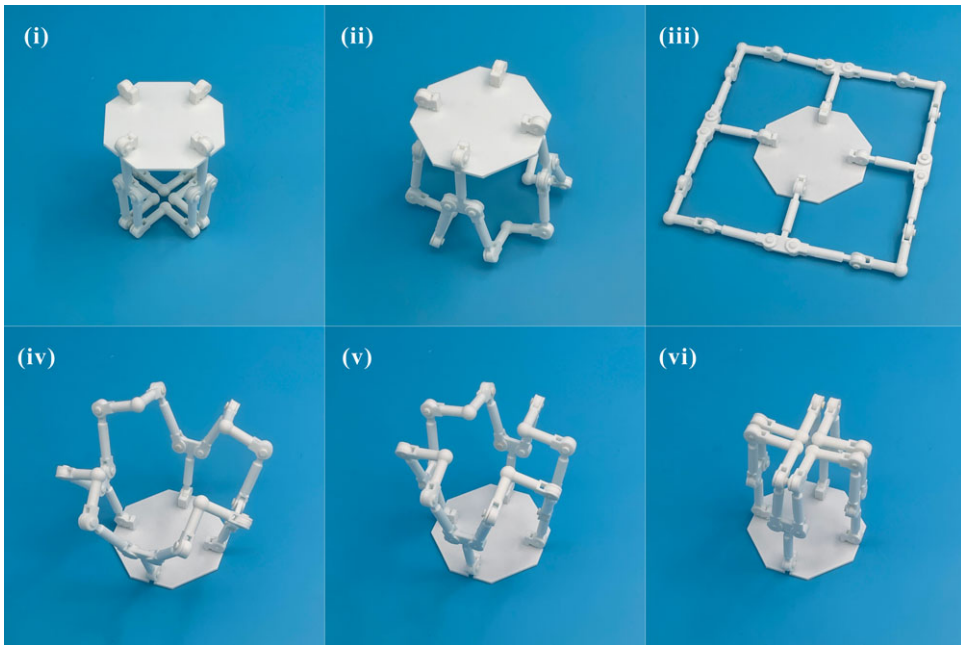


Figure 8. The folding sequence of a rigid gripper prototype.

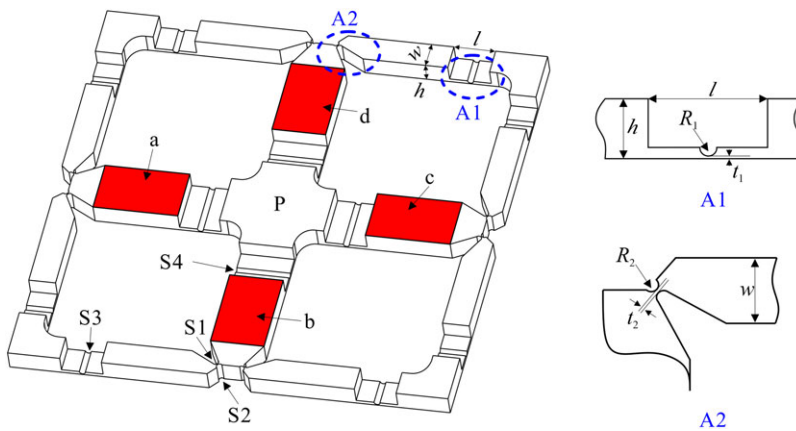


Figure 9. Structure diagram of the compliant gripper.

to zero, which indicates that the mechanism is grasping the target object tightly. When θ_2^1 approaches $\theta_{2d}^1 = 0.5\pi$, the distance among gripping points is the maximum, which indicates that the mechanism returns to the plane state. Further, kinematics equations of each Bricard linkage can be obtained as shown in Fig. 7(c)–7(e). Finally, a prototype was fabricated by 3D printing, where the design parameters are $\alpha = \frac{3\pi}{2}$, $\gamma = \frac{\pi}{2}$, $a = 54\text{mm}$, $r = 35\text{mm}$, $w = 20\text{mm}$. The folding process, see Fig. 8, shows that the mechanism can work with the ability to grasp.

4. A conceptual four-finger gripper

In the previous sections, the grasping possibility of the proposed network was shown by the kinematic study and the prototype of the network. To confirm the ability to grasp different shapes of objects and to

Table I. Flexure hinge variable level value.

Level Factor	Level-1 (mm)	Level-2 (mm)	Level-3 (mm)	Level-4 (mm)
<i>R</i>	1	1.5	2	2.5
<i>t</i>	0.2	0.25	0.3	0.35
<i>h</i>	5	6	7	8
<i>w</i>	7	8	9	10

Table II. The arrangement of experiment schemes.

Scheme	<i>R</i> (mm)	<i>t</i> (mm)	<i>h</i> (mm)	<i>w</i> (mm)	Scheme	<i>R</i> (mm)	<i>t</i> (mm)	<i>h</i> (mm)	<i>w</i> (mm)
1	1	0.2	5	7	9	2	0.2	7	10
2	1	0.25	6	8	10	2	0.25	8	9
3	1	0.3	7	9	11	2	0.3	5	8
4	1	0.35	8	10	12	2	0.35	6	7
5	1.5	0.2	6	9	13	2.5	0.2	8	8
6	1.5	0.25	5	10	14	2.5	0.25	7	7
7	1.5	0.3	8	7	15	2.5	0.3	6	10
8	1.5	0.35	7	8	16	2.5	0.35	5	9

Table III. Pressure values for simulations in ABAQUS.

Scheme	Stressed area (mm ²)	Force (N)	Pressure (MPa)	Scheme	Stressed (mm ²)	Force (N)	Pressure (MPa)
1	1764	24.5	0.0139	9	2240	24.5	0.0109
2	1920	24.5	0.0128	10	1980	24.5	0.0124
3	2052	24.5	0.0119	11	1984	24.5	0.0123
4	2160	24.5	0.0113	12	1708	24.5	0.0143
5	2124	24.5	0.0115	13	1792	24.5	0.0137
6	2400	24.5	0.0102	14	1652	24.5	0.0148
7	1596	24.5	0.0154	15	2320	24.5	0.0106
8	1856	24.5	0.0132	16	2196	24.5	0.0112

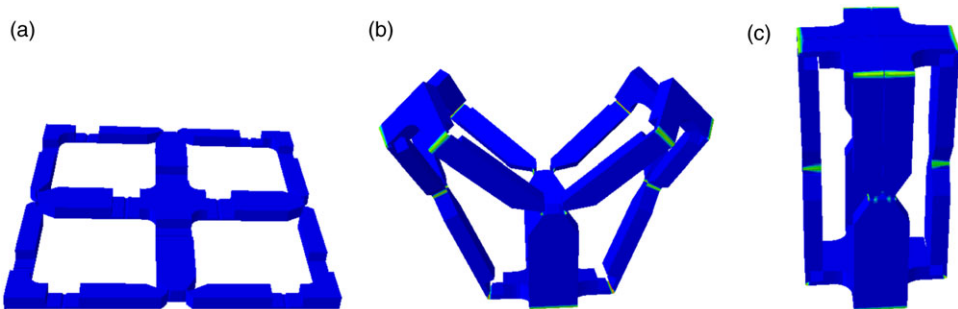


Figure 10. Static simulation of the compliant mechanism from (a) its planar configuration to (b) a middle folding process, and then to (c) the fully folded configuration.

Table IV. Experimental records from Minitab.

Scheme	σ_{\max_S1} (MPa)	σ_{\max_S2} (MPa)	σ_{\max_S3} (MPa)	σ_{\max_S4} (MPa)	σ_{\max} (MPa)
1	37.413	39.741	41.129	38.818	41.129
2	31.755	38.431	39.765	39.299	39.765
3	28.674	37.939	40.013	38.83	40.013
4	30.464	42.611	40.992	39.657	42.611
5	33.19	38.803	40.792	38.791	40.792
6	32.636	40.951	42.88	39.095	42.880
9	37.513	37.513	49.765	36.692	49.765
10	34.199	37.45	43.015	41.732	43.015
11	35.417	38.129	41.767	41.437	41.767
12	34.413	40.114	47.768	44.011	47.768
13	37.436	38.206	51.117	50.375	51.117
14	36.128	39.769	51.499	50.746	51.499
15	35.465	37.721	48.429	46.398	48.429

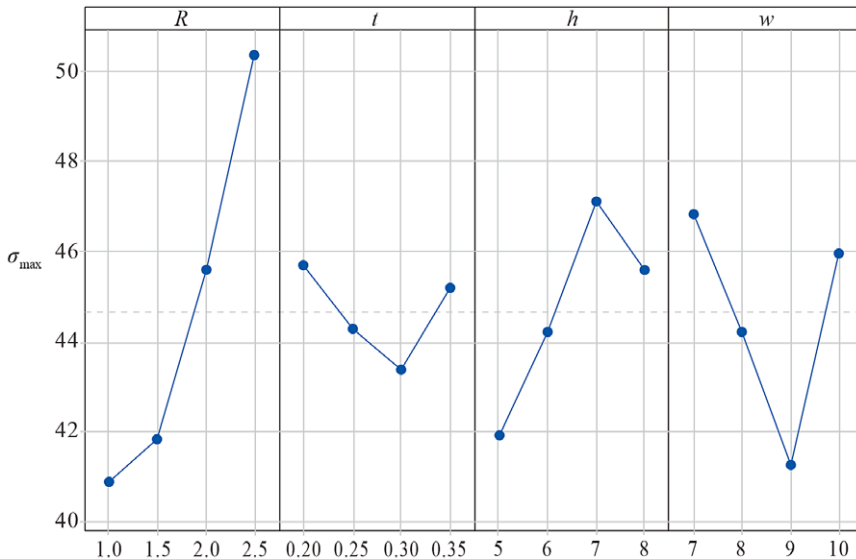


Figure 11. The result of the DOE Taguchi experiments.

show its advantage, the network will be realized with a compliant one as the skeleton of a gripper, and then the structural design, design parameters, and driven schemes will be discussed as follows.

4.1. The compliant mechanism

Based on the rigid gripper mechanism with the advantage of twist angle, this section adopts the rigid body replacement method [36] to transform the linkage into a compliant four-finger gripper mechanism, as shown in Fig. 9. The key to realize the design lies in the design of flexure hinges. Here, circular flexure hinges, which are easy to be manufactured, are adopted. According to the direction of the hinges in the mechanisms, there are two types, horizontal circular hinges and vertical circular ones, see A1, A2 in Fig. 9.

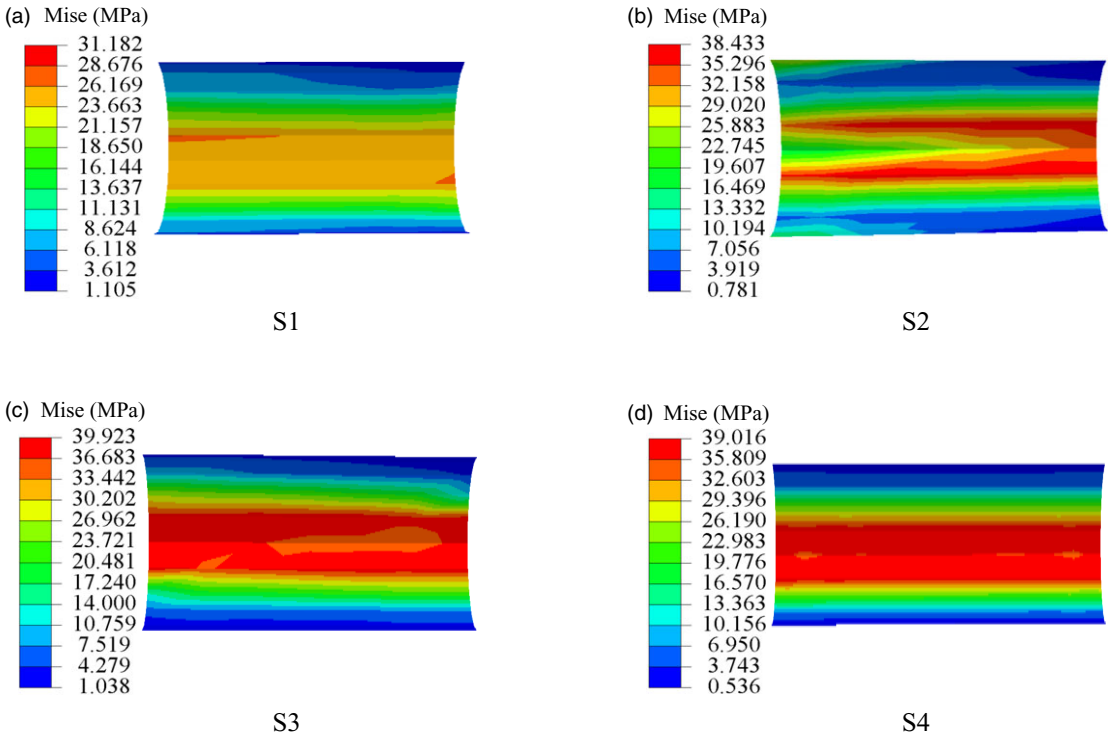


Figure 12. Stress situations of the optimized flexure hinge.

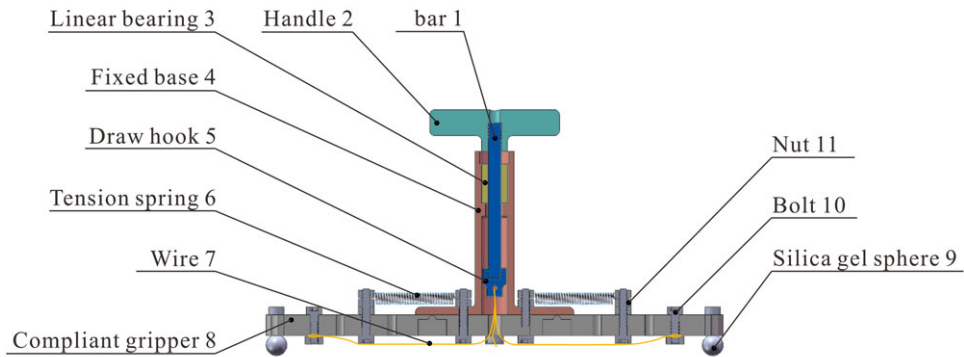


Figure 13. Schematic diagram of the cable-driven device.

In twofold-symmetric Bricard linkage, parameters a and r will affect the grasping range and do not affect the kinematics, here $a = 54$ mm and $r = 35$ mm are adopted. The arc radius R_1 of the horizontal circular hinge and its thickness t_1 , the arc radius R_2 of the vertical circular hinge and its thickness t_2 , the thickness of the plate h , and the distance of the adjacent Bricard linkage w are the design variables. Meanwhile, $l = 2h, R_1 = R_2 = R, t_1 = t_2 = t$ are satisfied to simplify the design and avoid physical interference, see Fig. 9.

4.2. Parameters of the flexible hinges

To obtain a set of reasonable parameters, DOE experiments are adopted based on static simulation. Here, R is set to the tool radius available on the market to facilitate future fabrication. Generally, t is located



Figure 14. Grasping process of the compliant gripper.

$0.05R \leq t \leq 0.8R$ [37]. Therefore, the DOE is set with four horizontal parameters listed in Table I, and then a group of 16 Taguchi experimental schemes with four factors is assigned in Table II.

PP plate, which exhibits great flexural fatigue resistance, with the density of 0.92 g/cm^3 , elastic modulus with 1620 MPa, and Poisson’s ratio with 0.4203, bending strength limit $\sigma_b = 56 \text{ MPa}$ is adopted, and simulations are performed in the implicit statics module of ABAQUS. Surface P is viewed as the fixed frame, and pressures are loaded on surfaces a, b, c, and d, see Fig. 9, whose values are listed in Table III to ensure the consistency of the driven forces.

After the simulations in ABAQUS, the results show that most schemes, except schemes 7, 8, and 16, could move from the plane configuration to the fully folded one under the action of the applied load to realize the grasping function, such as the result of scheme 3 in Fig. 10 as an example. The Mises stresses on hinge surfaces S1, S2, S3, and S4, whose locations are labeled in Fig. 9, are taken as the optimized metrics.

The Mises stresses of 13 groups of experiments are obtained from the results of the finite element analysis (FEA) in Table IV. Then, the analysis of experiment results was carried out in Minitab, and the influence of each parameter on the maximum stress value, σ_{\max} , is obtained, as shown in Fig. 11.

Therefore, the DOE experiment predicts that the compliant mechanism with $R = 1 \text{ mm}$, $t = 0.3 \text{ mm}$, $h = 5 \text{ mm}$, $w = 9 \text{ mm}$, will own smaller stresses, which is also verified by a further simulation with this set of parameters, as shown in Fig. 12. Meanwhile, the maximum stresses of the four hinge surfaces are $\sigma_{\max_S1} = 31.182 \text{ MPa}$, $\sigma_{\max_S2} = 38.433 \text{ MPa}$, $\sigma_{\max_S3} = 39.923 \text{ MPa}$, $\sigma_{\max_S4} = 39.016 \text{ MPa}$, all of which are smaller than the allowable stress by taking the safety factor $n_b = 1.3$,

$$[\sigma_b] = \frac{\sigma_b}{n_b} = \frac{56}{1.3} \approx 43.08 \text{ MPa}. \tag{17}$$

Hereby, a set of parameters $a = 45 \text{ mm}$, $r = 20 \text{ mm}$, $R = 1 \text{ mm}$, $t = 0.3 \text{ mm}$, $h = 5 \text{ mm}$, and $w = 9 \text{ mm}$ is determined, then a ball-end mill with a diameter of 2 mm and a flat-end cutter with a diameter of 2 mm were chosen to process the horizontal circular hinge and vertical circular hinge by an engraving machine, respectively.

4.3. Driven scheme

To cooperate with the proposed compliant mechanism, a cable-driven device, composed of four tension springs, a prismatic pair device and four pulling wires, is designed, as shown in Fig. 13.

A draw-bar and a linear bearing are used in the prismatic pair device, and the axial movement of the draw-bar is controlled by the handle to drive the gripper. One end of each tension spring is fixed to the bolted connection of the fixed base in the prismatic pair device, and the other end connects the compliant gripper with bolts. Wires are used to transmit the driven force by connecting the draw hook and the compliant mechanism. A cable-driven device was finally fabricated by 3D printing, and it can realize the grasping function by adjusting the height of the handle, see Fig. 14.

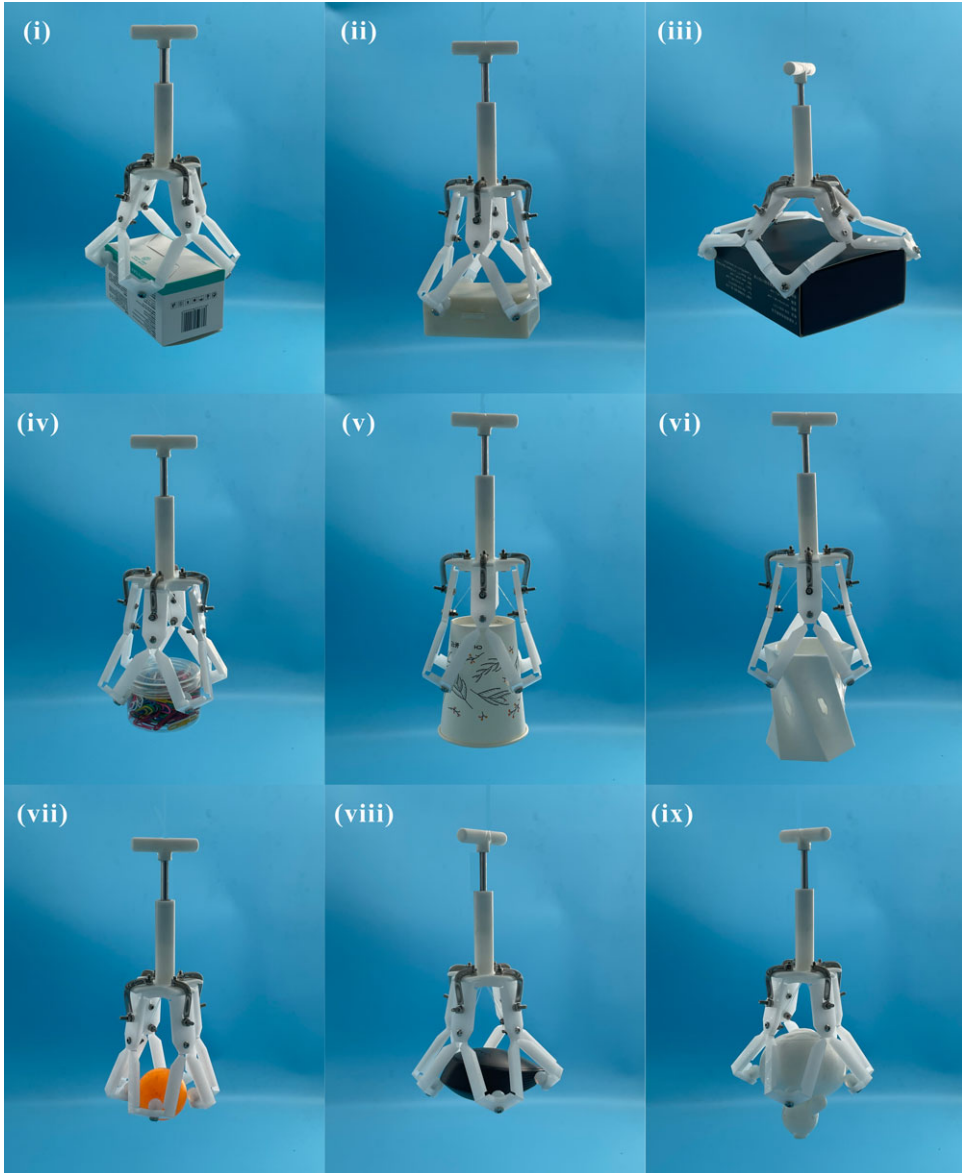


Figure 15. Grasping test of the compliant gripper.

To verify the grasping efficiency of the compliant gripper mechanism, some different shapes of objects, such as square-, cylinder-, spherical, and irregular bodies are selected for the grasping test, as shown in Fig. 15. It can be seen that the gripper has the advantages of simple structure, large working range and strong adaptability, and can grasp different types of articles.

5. Conclusions

In this paper, a novel gripper mechanism based on a compliant network with four identical twofold-symmetrical $6R$ linkages was proposed. The mobility is analyzed by the topological theory, and shows that the proposed network is with one DOF. The grasping potential was demonstrated with the folding

performance by the truss-transformation method, and the results are verified by a physical prototype. By the rigid body replacement method, a compliant four-finger gripper was designed and fabricated. Finally, the function of the compliant four-finger gripper was realized by a cable-driven scheme.

Compared with the existing grippers that can grasp objects with complex shapes, such as five-fingered humanoid robotic hand [7], underactuated robotic hand [18], SAU-RFC hand [19], etc., the compliant gripper proposed in this paper has the advantages of compact structure, single degree of freedom and low manufacturing cost, and owns lower stiffness due to the usage of compliant joints.

In the future, the design parameters of the flexure hinges will be optimized by the pseudo-rigid-body-model [30] to reduce the deformation stress. Due to the property of compliance, the deformation energy on compliant joints should be considered in the evaluation of grasping performance, and the grasping indices, such as G.I. index, C.I. index, and so forth [38], will be modified to fit compliant grippers.

Supplementary material. To view supplementary material for this article, please visit <https://doi.org/10.1017/S0263574722001503>.

Author contributions. FY, JZ, and LY conceived and designed the study. KC and TL conducted the derivation of equations, designed prototypes, and carried out the experiments. KC, TL, and FY wrote the draft of the article. FY, KC, TL, JZ, and LY revised the article.

Acknowledgement. The authors appreciate Mr. Weiwei Lin and Mr. Shuailong Lu for the help on the fabrication of the compliant mechanism and Mr. Yuan Gao for the assistance on the application of the truss-transformation method.

Financial support. This work was supported by the National Natural Science Foundation of China (Project No. 51905101), the Natural Science Foundation of Fujian Province, China (Project Nos. 2019J01209, 2020J06010), and Fuzhou University Testing Fund of Precious Apparatus (Project No. 2022T014).

Competing interests declaration. The authors declare none.

References

- [1] H. Kocabas, “Gripper design with spherical parallelogram mechanism,” *J. Mech. Des.* **131**(7), 075001 (2009).
- [2] Y. Lu, C. Zhang, C. Cao, Y. Dong and Y. Liu, “Kinematics and dynamics of a novel hybrid manipulator,” *Proc. Inst. Mech. Eng. C: J. Mech. Eng. Sci.* **230**(10), 1644–1657 (2016).
- [3] M. Honarpardaz, M. Tarkian, J. Olvander and X. Feng, “Finger design automation for industrial robot grippers: A review,” *Robot. Auton. Syst.* **87**, 104–119 (2017).
- [4] M. Maggi, G. Mantriota and G. Reina, “Introducing POLYPUS: A novel adaptive vacuum gripper,” *Mech. Mach. Theory* **167**(2), 104483 (2022).
- [5] X. Y. Zhou, H. P. Wang, Y. Tian and G. Zheng, “Disturbance observer-based adaptive boundary iterative learning control for a rigid-flexible manipulator with input backlash and endpoint constraint,” *Int. J. Adapt. Control Signal Process.* **34**(9), 1220–1241 (2020).
- [6] C. Yang, K. Huang, H. Cheng, Y. Li and C.-Y. Su, “Haptic identification by ELM-controlled uncertain manipulator,” *IEEE Trans. Syst. Man Cybern. Syst.* **47**(8), 2398–2409 (2017).
- [7] S. Mukherjee, A. Mahapatra, A. Kumar and A. Chatterjee, “Study of grasp-energy based optimal distribution of contact forces on a humanoid robotic hand during object grasp,” *Robotica* **40**(5), 1501–1526 (2022).
- [8] J. Shintake, V. Cacucciolo, D. Floreano and H. Shea, “Soft robotic grippers,” *Adv. Mater.* **30**(29), 1707035 (2018).
- [9] S. Abondance, C. B. Teeple and R. J. Wood, “A dexterous soft robotic hand for delicate in-hand manipulation,” *IEEE Robot. Autom. Lett.* **5**(4), 5502–5509 (2020).
- [10] W. Park, S. Seo and J. Bae, “A hybrid gripper with soft material and rigid structures,” *IEEE Robot. Autom. Lett.* **4**(1), 65–72 (2019).
- [11] X. J. Zhang and A. E. Oseyemi, “A herringbone soft pneu-net actuator for enhanced conformal gripping,” *Robotica* **40**(5), 1345–1360 (2022).
- [12] D. Cardin-Catalan, S. Ceppetelli, A. P. del Pobol and A. Morales, “Design and analysis of a variable-stiffness robotic gripper,” *Alex. Eng. J.* **61**(2), 1235–1248 (2022).
- [13] Z. F. Shang, J. Y. Ma, Z. You and S. Wang, “A foldable manipulator with tunable stiffness based on braided structure,” *J. Biomed. Mater. Res. B Appl. Biomater.* **108**(2), 316–325 (2019).
- [14] B. P. Mathew, F. Devasia, A. Asok, P. R. Jayadevu and R. Baby, “Implementation of an origami inspired gripper robot for picking objects of variable geometry,” *Mater. Today: Proc.* **58**, 176–183 (2022).
- [15] D. Jeong and K. Lee, “Design and analysis of an origami-based three-finger manipulator,” *Robotica* **36**(2), 261–274 (2017).

- [16] K. Zhang, Y. Zhu, C. Lou, P. Zheng and M. Kovač, “A Design and Fabrication Approach for Pneumatic Soft Robotic Arms Using 3D Printed Origami Skeletons,” *In: 2nd IEEE International Conference on Soft Robotics*, (IEEE, 2019).
- [17] C. Y. Liu, P. Maiolino and Z. You, “A 3D-printable robotic gripper based on thick panel origami,” *Front. Robot. AI* **8**(730227), 1–12 (2021).
- [18] R. K. Hota and C. S. Kumar, “Effect of design parameters on strong and immobilizing grasps with an underactuated robotic hand,” *Robotica* **40**, 1–17 (2022).
- [19] C. Su, R. Wang, T. Lu and S. Wang, “SAU-RFC hand: A novel self-adaptive underactuated robot hand with rigid-flexible coupling fingers,” *Robotica* **4**, 1–19 (2022).
- [20] Q. M. Marwan, S. C. Chua and L. C. Kwek, “Comprehensive review on reaching and grasping of objects in robotics,” *Robotica* **39**, 1–34 (2021).
- [21] C. Mavroidis and B. Roth, “New and revised overconstrained mechanisms,” *J. Mech. Des.* **117**(1), 75–82 (1995).
- [22] H. Shen, H. L. Huang and T. Ji, “Normalized-constrained approach for joint clearance design of deployable overconstrained Myard 5R mechanism,” *J. Adv. Mech. Des. Syst. Manuf.* **9**(5), 15-00386 (2015).
- [23] C. Y. Song, Y. Chen and I. Chen, “Kinematic study of the original and revised general line-symmetric Bricard 6R linkages,” *J. Mech. Robot.* **6**(3), 031002 (2014).
- [24] H. Feng, Y. Chen, J. S. Dai and G. Gogu, “Kinematic study of the general plane-symmetric Bricard linkage and its bifurcation variations,” *Mech. Mach. Theory* **116**(1), 89–104 (2017).
- [25] F. F. Yang and K. J. Chen, “General kinematic solutions of twofold-symmetric Bricard 6R linkage,” *J. Tianjin Univ* **54**(11), 1168–1178 (2021), in Chinese.
- [26] X. Song, H. Guo, R. Liu, F. Meng, Q. Chen, Y. Xu and R. Liu, “Mobility analysis of the threefold-symmetric Bricard linkage and its network,” *J. Mech. Robot* **12**(1), 011013 (2020).
- [27] D. Xu, E. Li, Z. Liang and Z. Gao, “Design and tension modeling of a novel cable-driven rigid snake-like manipulator,” *J. Intell. Robot. Syst.* **99**(2), 211–228 (2020).
- [28] K. J. Chen, F. F. Yang and J. Zhang, “Kinematics of a One-DOF Four-Finger Gripper Constructed with Two-Fold Symmetric Bricard Linkages,” *In: The 14th International Conference on Intelligent Robotics and Applications*, Yantai, China, ICIRA, Part III, LNAI 13015 (2021) pp. 728–738.
- [29] J. Denavit and R. S. Hartenberg, “A kinematic notation for lower-pair mechanisms,” *ASME J. Appl. Mech.* **22**(2), 215–221 (1955).
- [30] L. L. Howell and A. Midha, “A loop-closure theory for the analysis and synthesis of compliant mechanisms,” *ASME J. Mech. Des.* **118**(1), 121–125 (1996).
- [31] K. Wohlhart, “Screw Spaces and Connectivities in Multiloop Linkages,” *In: 9th International Symposium on Advances in Robot Kinematics*, Springer, Sestri Levante, Italy (2004) pp. 97–104.
- [32] J. S. Dai, “Finite displacement screw operators with embedded chasles’ motion,” *J. Mech. Robot.* **4**(4), 041002 (2012).
- [33] F. Yang, Y. Chen, R. Kang and J. Ma, “Truss transformation method to obtain the non-overconstrained forms of 3D overconstrained linkages,” *Mech. Mach. Theory* **102**, 149–166 (2016).
- [34] S. Pellegrino and C. R. Calladine, “Matrix analysis of statically and kinematically indeterminate frameworks,” *Int. J. Solids Struct.* **22**(4), 409–428 (1986).
- [35] P. Kumar and S. Pellegrino, “Computation of kinematic paths and bifurcation points,” *Int. J. Solids Struct.* **37**(46-47), 7003–7027 (2000).
- [36] L. L. Howell and A. Midha, “A method for the design of compliant mechanisms with small-length flexural pivots,” *Trans. ASME* **116**(1), 280–290 (1994).
- [37] Y. K. Yong, T. F. Lu and D. C. Handley, “Review of circular flexure hinge design equations and derivation of empirical formulations,” *Precis. Eng.* **32**(2), 63–70 (2008).
- [38] G. Carbone. *Grasping in Robotics* (Springer, London, Heidelberg, New York, Dordrecht, 2012).